IDEAL-VISCOPLASTIC EXTRUSION MODEL

C.P.T. Groth* and J.J. Gottlieb

Institute for Aerospace Studies
University of Toronto
Downsview, Ontario
M3H 5T6, Canada

Received November, 1990, accepted October, 1991
No. 90-CSME-33, EIC Accession No. 2260

ABSTRACT

An approximate one-dimensional analysis is presented for the extrusion of incompressible ideal-viscoplastic material through converging axisymmetric dies. The extrusion model incorporates the fundamental effects of inertia, plastic deformation, strain-rate behaviour, and surface friction by employing the constitutive relations for a Bingham-type body to describe the stress-strain-rate behaviour of the extrudite, an appropriate quasi-steady locally-spherical kinematically-admissible velocity field to represent the actual flow field, and a combination Coulomb and constant-shear-factor laws to estimate the frictional forces along the die surface. Comparisons of the predictions of the theory to experimental data and finite-element computations demonstrate that it is a useful and economical tool for predicting many extrusion processes.

Modélisation de l'extrusion viscoplastique

Une analyse unidimensionnelle de l'extrusion d'un matériau viscoplastique idéal et incompressible à travers des moules convergents et axisymétriques est proposée dans cet article. Le modèle incorpore les effets de l'inertie, de la déformation plastique, du comportement contraintes-déformations et de la friction de contact en utilisant les équations constitutives pour un corps de type Bingham, afin de décrire les comportements liés aux taux de déformation du matériau; un champ de vélocité approprié, quasi-permanent, local-sphérique et cinématiquement admissible pour représenter le domaine d'écoulement réel; et une combinaison des lois de Coulomb et des facteurs de cisaillement constant afin d'estimer les forces de friction le long de la surface du moule. Des comparaisons entre cette théorie et des données expérimentales, et avec des modélisations par éléments finis, montrent que cette méthode est utile et économique pour prédire plusieurs procédés d'extrusion.

*Research Assistant

INTRODUCTION

Extrusion or drawing is a prevalent process common to many technological metal and thermoplastic forming procedures associated with large permanent deformations, such as wire drawing, rod extrusion, hydrostatic extrusion, and tube sinking [1–5]. A cylindrical wire, rod, or tube is usually the product of these manufacturing processes.

During the extrusion process, material is shaped or formed by forcing it through a converging channel or die. The forces required for extrusion are large and the combined state of stress within the extruding material reaches the plastic yield limit, above which permanent plastic deformation occurs. A typical arrangement is depicted in Fig. 1.

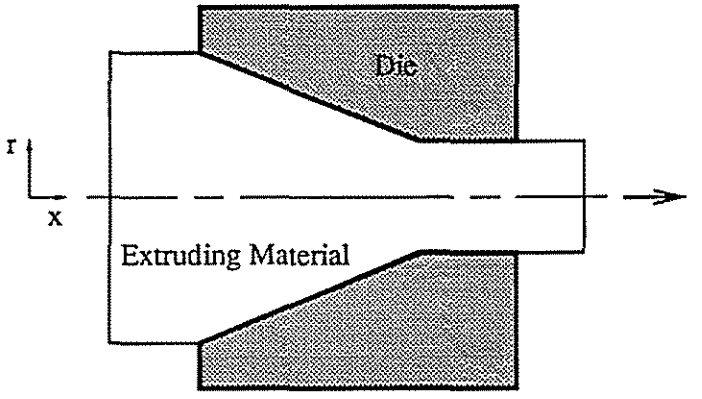

Fig. 1. Illustration of extrusion of a material forced through a converging channel.

The general extrusion process is a complicated three-dimensional problem with six different components of stress and three velocity or strain-rate components requiring a representative equation set with a minimum of three motion equations and six constitutive (stress-strain) relations. Consequently, a general mathematical theory for predicting the motion of an extruding material, the forces associated with that motion, and the stresses and forces exerted on the die or channel during the process can become very complex, and exact solutions are not available. For these reasons, previous theoretical studies have resorted to simplified analyses.

One of the first analytic models developed to describe the deformation forces associated with extrusion processes was proposed by von Kármán, Hencky, Siebel, and later by Sachs in the 1920s [1, 4, 6]. This early model considered only plastic deformation forces and neglected strain-rate behaviour. Subsequently, in the 1940s and 1950s, researchers such as Hill [7], Johnson [8], Jordan and Thomsen [9], and Prager [10] used slip-line theory to study the extrusions of metal through various die geometries. During this same time period, Shield [11] published semi-analytic solutions for the equilibrium flows of ideal-plastic materials in conical channels, with both von Mises and Tresca yield criteria. Later, another mathematical technique, the theory of limit analysis [1–3, 10, 12], was widely used to analyze plastic deformation processes. By employing the theory of limit analysis, Avitzur [1, 3] derived an upper-bound solution for the stress fields in ideal-plastic materials extruded through conical converging dies. In another study, Leech [13] developed an

approximate theory for high-speed extrusions, in which inertial and surface-normal (pressure) forces dominate. More recently, Cristescu [14, 15] has developed an approximate analysis for the extrusion process through conical converging dies which included the effects of plastic deformation, strain-rate behaviour, and friction.

All of these aforementioned analytic or semi-analytic solutions to the extrusion problem were derived by making certain valid but restrictive physical assumptions. Although they can provide many useful results, each of these models fails to incorporate all of the important physical features of the process (i.e., inertial, strain, strain-rate, and frictional effects) into a cohesive analysis.

In the past 20 years, numerical methods have superseded analytic techniques in many areas. Much attention has been devoted to obtaining solutions to complex problems in dynamics, such as the extrusion process, by using powerful numerical techniques. The finite-element method [16, 17] has been adapted and used extensively to solve many problems related to the dynamic response of linear and nonlinear continua with complex geometries and boundary conditions, as well as realistic material properties. Finite-element computer programs are available that incorporate the effects of inertia, elastic and plastic strain, strain-rate behaviour, and friction in problems involving large permanent deformations [18]. Although these computer programs are being used for extrusion analyses, a comprehensive and often computationally expensive numerical study is not always warranted, particularly in many design applications.

In this paper the extrusion problem is reconsidered. A semi-analytic and approximate one-dimensional model for the extrusion of ideal-viscoplastic materials is derived. This model generalizes and extends the work of Cristescu [14,15] to include inertial, plastic strain, strain-rate, and frictional effects for the more general case of axisymmetric converging channels. Comparisons of the theoretical solutions to actual experimental extrusion data, as well as finite-element method predictions, show that the analysis is a useful and practical tool for predicting the motion of extruding materials. Furthermore, it does not require unduly complicated or expensive computational techniques.

EQUATIONS OF MOTION

Assuming that the die is rigid, the extrudite is incompressible, and the extrusion process is isothermal and axisymmetric, the general continuity and radial and axial momentum equations for continuous deformable mediums can be written as

$$\frac{1}{r}\frac{\partial}{\partial r}(ru_r) + \frac{\partial u_x}{\partial x} = 0\,, \tag{1}$$

$$\rho\left[\frac{\partial u_r}{\partial t} + u_r\frac{\partial u_r}{\partial r} + u_x\frac{\partial u_r}{\partial x}\right] = f_r + \frac{\partial \sigma_{rr}}{\partial r} + \frac{\sigma_{rr} - \sigma_{\theta\theta}}{r} + \frac{\partial \sigma_{xr}}{\partial x}\,, \tag{2}$$

$$\rho\left[\frac{\partial u_x}{\partial t} + u_r\frac{\partial u_x}{\partial r} + u_x\frac{\partial u_x}{\partial x}\right] = f_x + \frac{\partial \sigma_{xx}}{\partial x} + \frac{\partial \sigma_{xr}}{\partial r} + \frac{\sigma_{xr}}{r}\,, \tag{3}$$

where ρ, u_r, u_x, r, x, f_r, and f_x are the density, radial and axial components of velocity, position coordinates, and body forces per unit volume, respectively. The surface stress variables σ_{rr}, σ_{xx}, and $\sigma_{\theta\theta}$ are the radial, axial, and azimuthal or circumferential components of the normal strain and

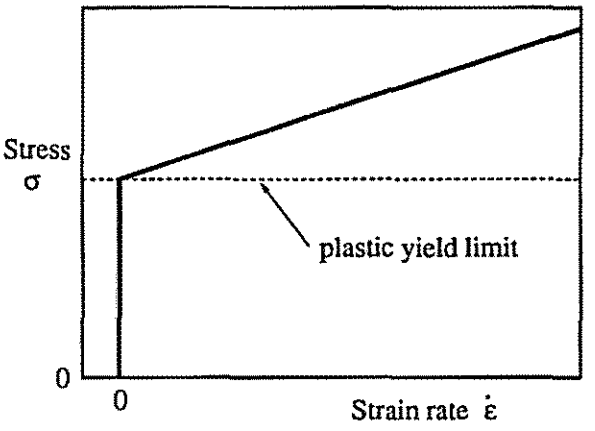

Fig. 2. Stress versus strain rate for a typical Bingham body exhibiting ideal-viscoplastic behaviour.

σ_{xr} is the component of shear stress in the axial-radial plane. In arriving at these equations it is assumed that there is no rotational motion about the axis of symmetry.

In order to complete Eqs. (1)–(3), the surface stresses σ_{rr}, σ_{xx}, $\sigma_{\theta\theta}$, and σ_{xr} must be specified. These stresses are intimately dependent on the state of strain of the deforming material, and a set of constitutive relations is usually used to relate the stresses to the corresponding strains. Constitutive relationships are empirical in nature and attempt to represent the macroscopic deformation of a material subjected to a particular state of stress, without examining the microscopic mechanisms in detail [19, 20].

Due to the diversity of materials and their related properties, there are a large number of constitutive or stress-strain relations that have been documented in the open literature. For this study, it is appropriate to assume that the material is homogeneous. Furthermore, most extrusion processes are virtually incompressible (isochoric) and feature permanent plastic deformation and large strain. In such cases, the deformation energy associated with plastic strain is very much larger than the elastic-strain energy and it is therefore appropriate to neglect elastic effects [10]. In addition, Cristescu [14, 15] has shown that strain-rate effects are significant in the drawing process, particularly if the diameter of the final product is small. For these reasons, the stress/strain-rate relations describing an isotropic ideal-viscoplastic body [14, 15, 21–25] are used here.

The ideal-viscoplastic medium, often referred to as a Bingham body, remains rigid in the elastic range, exhibiting no strain below the well-known Huber-Mises or von Mises yield criterion, and then deforms as an ideal Newtonian viscous fluid once the plastic yield limit has been reached. Elastic strain is completely absent in this incompressible material. This stress/strain-rate response is depicted in Fig. 2.

The general ideal-viscoplastic constitutive relations can be written in the following form using the usual tensor notation:

$$\dot{\epsilon}_{ij} = \begin{cases} 0 & \sigma_{eq} < Y\,, \\ \left[\dfrac{1}{\lambda} + \eta\right]^{-1} (\sigma_{ij} - \delta_{ij}\sigma_m) = \dfrac{1}{\eta}\left[1 - \dfrac{Y}{\sigma_{eq}}\right] s_{ij} & \sigma_{eq} \geq Y\,, \end{cases} \tag{4}$$

with the additional equations

$$\sigma_m = \frac{1}{3}\sum_i \sigma_{ii} = \frac{\sigma_{11}+\sigma_{22}+\sigma_{33}}{3} = -p\,, \tag{5}$$

$$\lambda = \frac{\dot{\epsilon}_{eq}}{Y} = \frac{1}{\sqrt{2}Y}\left[(\dot{\epsilon}_{11}-\dot{\epsilon}_{22})^2+(\dot{\epsilon}_{22}-\dot{\epsilon}_{33})^2+(\dot{\epsilon}_{33}-\dot{\epsilon}_{11})^2+6(\dot{\epsilon}_{12}^2+\dot{\epsilon}_{23}^2+\dot{\epsilon}_{31}^2)\right]^{1/2}, \tag{6}$$

$$\begin{aligned}\sigma_{eq} &= \frac{1}{\sqrt{2}}\left[(\sigma_{11}-\sigma_{22})^2+(\sigma_{22}-\sigma_{33})^2+(\sigma_{33}-\sigma_{11})^2+6(\sigma_{12}^2+\sigma_{23}^2+\sigma_{31}^2)\right]^{1/2}, \\ &= \sqrt{\frac{3}{2}}\left[s_{11}^2+s_{22}^2+s_{33}^2+2(s_{12}^2+s_{23}^2+s_{31}^2)\right]^{1/2}. \end{aligned} \tag{7}$$

In Eqs. (4)–(7), σ_{ij} and $\dot{\epsilon}_{ij}$ are the respective stress and strain-rate tensors, s_{ij} is the deviatoric stress tensor, σ_m is the mean or hydrostatic stress defined by Eq. (5), p is the pressure, and δ_{ij} is the Kronecker delta function. The deviatoric and generalized stress tensors s_{ij} and σ_{ij} can be related by $s_{ij} = \sigma_{ij} - \delta_{ij}\sigma_m = \sigma_{ij} + \delta_{ij}p$. The variables η and λ are the viscosity and plastic deformation proportionality coefficients, respectively. The former variable is a material constant and the latter variable is dependent on the state of strain and is defined by Eq. (6), where $\dot{\epsilon}_{eq}$ is the equivalent or effective strain rate. Finally, Y is the tensile yield strength of the material and σ_{eq} is the equivalent or effective combined stress defined by Eq. (7). Note that $\sigma_{eq} = Y + \eta\dot{\epsilon}_{eq}$ for $\sigma_{eq} \geq Y$.

The stress-strain relations of Eq. (4) can be thought of as a combination of the classical Levy-Mises equations for ideal-plastic bodies [6, 7, 10, 19, 26] and the traditional Stokes laws for ideal viscous fluids [20]. The equations assert that once the plastic yield criterion is reached (i.e., $\sigma_{eq} \geq Y$), the total stress in the material is then the sum of the ideal-plastic shear stress, viscous shear stress, and mean (hydrostatic) stress. Below the plastic yield point ($\sigma_{eq} < Y$) the strain rates are zero and the material behaves as a rigid body. In the latter case, the stress distribution must be determined from a consideration of the material loading and dynamics. The Huber-Mises or von Mises yield criterion of Eq. (6) is often used to study plastic deformation of many isotropic materials. This criterion postulates that the onset of plastic flow is precipitated by the shear stresses and governed by the total shear energy reaching some critical value [6, 7, 10, 19, 26].

By using the stress/strain-rate equations described above and relating the strain rates $\dot{\epsilon}_{ij}$ to gradients of the velocity field [20, 27], expressions for the four axisymmetric strain-rate components in terms of the associated deviatoric stresses s_{rr}, s_{xx}, $s_{\theta\theta}$, and s_{xr} can be written as

$$\dot{\epsilon}_{rr} = \frac{\partial u_r}{\partial r} = \begin{cases} 0 & \sigma_{eq} < Y\,, \\ \left[\dfrac{1}{\lambda}+\eta\right]^{-1} s_{rr} & \sigma_{eq} \geq Y\,, \end{cases} \tag{8}$$

$$\dot{\epsilon}_{xx} = \frac{\partial u_x}{\partial x} = \begin{cases} 0 & \sigma_{eq} < Y\,, \\ \left[\dfrac{1}{\lambda}+\eta\right]^{-1} s_{xx} & \sigma_{eq} \geq Y\,, \end{cases} \tag{9}$$

$$\dot{\epsilon}_{\theta\theta} = \frac{u_r}{r} = \begin{cases} 0 & \sigma_{eq} < Y, \\ \left[\frac{1}{\lambda} + \eta\right]^{-1} s_{\theta\theta} & \sigma_{eq} \geq Y, \end{cases} \tag{10}$$

$$\dot{\epsilon}_{xr} = \frac{1}{2}\left(\frac{\partial u_r}{\partial x} + \frac{\partial u_x}{\partial r}\right) = \begin{cases} 0 & \sigma_{eq} < Y, \\ \left[\frac{1}{\lambda} + \eta\right]^{-1} s_{xr} & \sigma_{eq} \geq Y, \end{cases} \tag{11}$$

where the plastic deformation coefficient is given by

$$\lambda = \frac{\sqrt{3}}{\sqrt{2}Y}\left[\left(\frac{\partial u_r}{\partial r}\right)^2 + \left(\frac{u_r}{r}\right)^2 + \left(\frac{\partial u_x}{\partial x}\right)^2 + \frac{1}{2}\left(\frac{\partial u_r}{\partial x} + \frac{\partial u_x}{\partial r}\right)^2\right]^{1/2}, \tag{12}$$

and the equivalent stress can be expressed as

$$\sigma_{eq} = \sqrt{\frac{3}{2}}\left[s_{rr}^2 + s_{\theta\theta}^2 + s_{xx}^2 + 2s_{xr}^2\right]^{1/2}. \tag{13}$$

In the preceding equations, $\dot{\epsilon}_{rr}$, $\dot{\epsilon}_{xx}$, and $\dot{\epsilon}_{\theta\theta}$ are the radial, axial, and azimuthal components of normal strain rate and $\dot{\epsilon}_{xr}$ is the shear strain rate in the axial-radial plane.

Equations (8)–(13) describe the stress field in an ideal-viscoplastic axisymmetric body. Frictional forces arising from the interaction of the extruding material and channel wall can have a predominant effect on the magnitude of these stresses. These frictional effects enter the analysis by means of boundary conditions for the wall shear stress. In this study, a combination of the well-known classical law of friction, often referred to as Amontons or Coulombs law [28, 29], and the widely used constant shear factor model [2, 3, 4, 14] is used to prescribe the wall shear stress as follows:

$$\tau_f = \begin{cases} S(V)\mu\sigma_n & |\mu\sigma_n| < \frac{mY}{\sqrt{3}}, \\ -S(V)\frac{mY}{\sqrt{3}} & |\mu\sigma_n| \geq \frac{mY}{\sqrt{3}}, \end{cases} \tag{14}$$

and

$$\mu = \begin{cases} \mu_s & |V| \leq V_o, \\ \mu_k + (\mu_s - \mu_k)\exp\left[-\beta(|V| - V_o)\right] & |V| > V_o, \end{cases} \tag{15}$$

where τ_f is the wall shear stress, σ_n is the local normal stress acting on the surface, Y is the tensile yield stress of the extruding material, m is the maximum frictional shear stress proportionality constant ($0 \leq m \leq 1$), μ is the coefficient of friction, and μ_s and μ_k are the related static and kinematic coefficients of friction respectively. V is the relative velocity of sliding contact and V_o and β are a reference velocity and a velocity decay parameter used to describe the variation of the coefficient of friction. $S(x)$ is the sign function which can take on values of $+1$ or -1 depending on

the sign of the argument x. The values of the variables m, μ_s, μ_k, V_o, and β depend on the properties of the materials in contact. For stresses below the maximum frictional shear stress $mY/\sqrt{3}$, the frictional stress τ_f as prescribed by Amontons law is the product of the coefficient of friction and the component of stress acting normal to the surface of contact. When this formulation for the frictional stress exceeds the maximum shear limit, τ_f is simply assigned the maximum value.

The friction coefficient used in Eq. (14) is an exponential function of the velocity of sliding contact as given by Eq. (15). It takes on values from the static value μ_s, for velocities in the range from zero up to the reference velocity, and asymptotically approaches the kinematic value μ_k at higher velocities. This relationship for the coefficient of friction is very similar to an expression proposed by Kragelsky, Dobychin, and Kombalov [28], and it is in general agreement with some very high-speed experimental data of Bowden and Freitag [30]. Another similar power-law expression for the friction coefficient has been used by Powell, Winstead, DeWitt, and Cable [31, 32] in their studies of piston and projectile wear in two-stage light-gas guns.

SIMPLIFYING ASSUMPTIONS

Rather than solve the set of nonlinear partial differential equations describing the extrusion of ideal-viscoplastic materials through axisymmetric converging channels given by Eqs. (1)–(3) and (8)–(15) by means of a complex numerical procedure, an approximate semi-analytic solution is sought by simplifying the governing equations and reducing them to a single ordinary differential equation with some ancilliary algebraic expressions. The following assumptions are employed:

(i) The area gradient of the converging channel is small (i.e., $\frac{1}{A}(\frac{dA}{dx})^2 \ll 1$, where the cross-sectional area A is a function of the axial coordinate x, $A = A(x)$).

(ii) The flow field of the extruding material is described by a *locally-spherical* quasi-steady *kinematically-admissible* velocity field such that the axial and radial velocity components are completely specified in terms of the channel geometry and mass flow rate.

(iii) The radial component of linear momentum is small compared to the axial momentum component (i.e., $u_r/u_x \ll 1$). On this premise, the radial momentum equation is no longer required for the analysis.

(iv) Frictional forces are included as an equivalent axial body force per unit volume.

In contrast to solving the complete two-dimensional equations, the radial momentum equation is dropped from the analysis and a kinematically-admissible velocity field is chosen to satisfy flow continuity and boundary conditions. This provides approximate expressions for the inertial and ideal-viscoplastic stress terms of the axial momentum equation. This equation is then reduced to an ordinary differential equation and can be used to predict the time evolution of the approximate velocity field. Obviously, the more accurately the kinematically-admissible velocity field approximates the actual flow field the better the model will be able to predict extrusion motion.

A *locally-spherical* kinematically-admissible velocity field is used herein. It is an approximate axisymmetric extension of the spherical velocity field used by Avitzur [1–3] and Cristescu [14, 15] in their studies of extrusions through conical converging channels with spherical symmetry. These

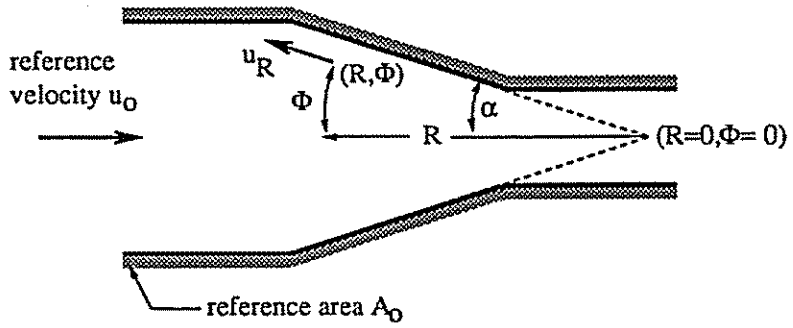

Fig. 3. Spherical velocity field for extrusion through a conical convergence.

studies indicate that the spherical velocity field used in conjunction with an upper-bound solution analysis is very appropriate for predicting extrusion forces as well as optimal die angles for the case of conical converging channels. The results of their studies provide partial justification for the use of such a velocity field here. The spherical velocity field is depicted in Fig. 3 and can be described at each point within the channel by the following equations:

$$u_R = \frac{-u_o A_o}{\pi \sin^2 \alpha} \frac{\cos \Phi}{R^2}, \tag{16}$$

$$u_\Phi = u_\Psi = 0, \tag{17}$$

where u_R, u_Φ, and u_Ψ are the radial and two angular components of the velocity vector. The radial velocity is dependent on the radius R and angle Φ of the spherical coordinate system. Note that the origin of this spherical coordinate frame of reference is located at the projected apex of the conical channel and the flow is symmetric with respect to the angular coordinate Ψ.

The other variables appearing in Eq. (16) are the reference velocity u_o and reference area A_o (defined in a constant-area section of the channel), as well as the semi-angle α of the conical area-reduction section (see Fig. 3). The term $-(u_o A_o)/(\pi \sin^2 \alpha)$ is a time-dependent parameter that is related to the instantaneous mass flow and channel geometry (i.e., it can be obtained by equating the mass flow rate for constant-area section of the channel to the mass flow rate through the area-reduction).

The extension of the spherical kinematically-admissible velocity field to the axisymmetric case is obtained on the premise that the flow at every point within the axisymmetric channel is *locally spherical* and thus directed towards an apex or origin defined by the local area gradient (i.e., tangent to channel wall). This locally-spherical flow field is illustrated in Fig. 4. Referring to the geometry shown therein, any location (x, r) in the area-reduction section of an axisymmetric channel is located on a radial arc whose origin is located at the intersection of the axis of symmetry with the line tangent to the channel wall. The radius of this arc is $R^2 = \hat{r}^2 + \hat{d}^2$, where $\hat{x}$ and $\hat{r}$ are the coordinates of the point of intersection of the arc and channel wall, and $\hat{d}$ is the distance along the axis of symmetry from point $(\hat{x}, \hat{r})$ to the local origin. The point $(\hat{x}, \hat{r})$ is the tangent point used to define the location of the origin for the arc.

All points in the flow located on the arc of radius R are assumed to have a velocity vector that is directed towards the local origin or apex of the arc with a magnitude defined by Eq. (16).

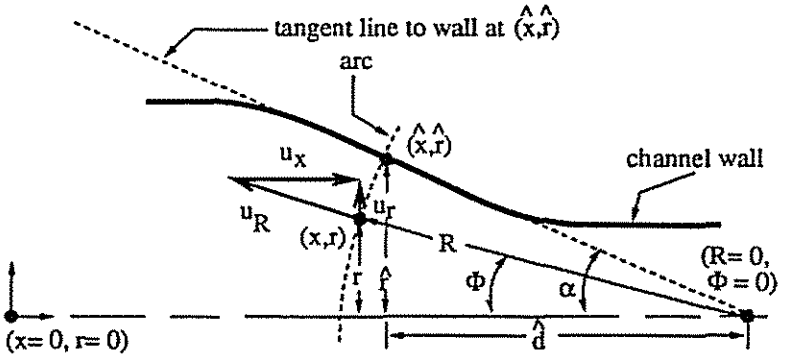

Fig. 4. Locally-spherical velocity field for extrusion through an axisymmetric area reduction.

By using geometrical considerations to relate R, Φ, and α to x, r, $\hat{x}$, $\hat{r}$, and $\hat{d}$, and then noting that axial and radial velocity components in an axisymmetric reference frame are merely the orthogonal components of the radial velocity component defined in a spherical frame, the radial and axial components of the locally-spherical kinematically-admissible velocity field may be written as

$$u_r = u_R \sin\Phi = \frac{-u_o A_o}{\pi} \frac{r(\hat{x} - x + \hat{d})}{\hat{r}^2(\hat{r}^2 + \hat{d}^2)}, \tag{18}$$

$$u_x = -u_R \cos\Phi = \frac{u_o A_o}{\pi} \frac{(\hat{x} - x + \hat{d})^2}{\hat{r}^2(\hat{r}^2 + \hat{d}^2)}. \tag{19}$$

Equations (18) and (19) define the locally-spherical flow field in terms of the variables x, r, $\hat{x}$, $\hat{r}$, and $\hat{d}$. Geometrical relationships can be used to relate $\hat{x}$, $\hat{r}$, and $\hat{d}$ to x and r. They are as follows:

$$\hat{r}^2 = \frac{\hat{A}}{\pi}, \tag{20}$$

$$\hat{d} = \frac{-2\hat{A}}{\dfrac{d\hat{A}}{dx}}, \tag{21}$$

$$\hat{r}^2 + \hat{d}^2 = r^2 + (\hat{x} - x + \hat{d})^2, \tag{22}$$

where $\hat{A} = A(\hat{x})$. Having done this, by applying Eqs. (20)–(22), making appropriate first-order linearizations using Taylor series expansions for $\hat{A}$ about x and the binomial theorem (assuming $(\hat{x} - x)dA/dx$ is small), and then simplifying, the following equation for $\hat{x}$ in terms of x, A, and r can be obtained and written as

$$\hat{x}^2 \approx x - \frac{1}{4\pi}\frac{dA}{dx}\left(1 - \frac{\pi r^2}{A}\right). \tag{23}$$

Approximate equations for the axial and radial components of the locally-spherical velocity field can then be obtained and expressed as

$$u_x = \frac{u_o A_o}{A}\left[1 - \frac{r^2}{2A^2}\left(\frac{dA}{dx}\right)^2 + \frac{1}{4\pi A}\left(\frac{dA}{dx}\right)^2\right], \tag{24}$$

$$u_r = \frac{u_o A_o}{2A^2}\frac{dA}{dx} r. \tag{25}$$

It should be emphasized that the velocity field described by Eqs. (24) and (25) is not an exact solution to the governing equations for extrusions, but it is instead an approximation to the exact velocity field that permits a simplification of the analysis. An indication of just how well the locally-spherical kinematically-admissible flow field appears to model the actual velocity field is given in the latter sections of this paper.

Once Eqs. (24) and (25) are assumed, the stress field as well as the boundary conditions for stresses along the die surface are prescribed by the ideal-viscoplastic constitutive equations. However, this stress field is an approximate solution only. The surface friction boundary conditions of Eqs. (14) and (15) are not taken into account by the kinematically-admissible velocity field. In addition, the stress field boundary conditions defined by Eqs. (24) and (25) are generally not representative of the actual frictional shear strains present very close to the surface of contact between the extruding material and channel. In order to include these effects, the frictional shear forces are treated as an additional body force per unit volume acting in the axial direction.

By applying the first assumption concerning small area gradients, an elemental volume of the axisymmetric duct can be approximated by elemental cylindrical disks of radius $r = \sqrt{A/\pi}$ and thickness Δx. The wall frictional shear stresses produce axial forces that act on this cylindrical volume element in a direction opposite to the flow. The net radial force of friction is zero. By employing Eqs. (14) and (15), approximating the stress normal to the channel-material interface σ_n by the radial stress σ_{rr} component, approximating the velocity of sliding contact V by the axial velocity u_x evaluated at the wall, and noting that the surface area of the elemental volume is $2\sqrt{\pi A}\Delta x$, the frictional body force per unit volume f_f acting in the axial direction can be expressed as

$$f_f = \begin{cases} S(u_o) 2\mu\sqrt{\dfrac{\pi}{A}}\,\sigma_{rr} & |\mu\sigma_{rr}| < \dfrac{mY}{\sqrt{3}}, \\ -S(u_o) 2m\sqrt{\dfrac{\pi}{3A}}\,Y & |\mu\sigma_{rr}| \geq \dfrac{mY}{\sqrt{3}}, \end{cases} \tag{26}$$

where the coefficient of friction is defined by

$$\mu = \begin{cases} \mu_s & \dfrac{|u_o| A_o}{V_o A} \leq 1. \\ \mu_k + (\mu_s - \mu_k)\exp\left[-\beta\left(\dfrac{|u_o| A_o}{A} - V_o\right)\right] & \dfrac{|u_o| A_o}{V_o A} > 1. \end{cases} \tag{27}$$

APPROXIMATE SOLUTION

An approximate solution for the extrusion of ideal-viscoplastic materials may now be developed from the simplifying assumptions presented in the previous section in conjunction with Eqs. (1)–(3) and (8)–(15). From Eqs. (24) and (25), the axial and radial velocity components for the extrusion process can be defined by

$$u_x = \begin{cases} \dfrac{u_o A_o}{A} & \dfrac{dA}{dx} \geq 0, \\ \dfrac{u_o A_o}{A}\left[1 - \dfrac{r^2}{2A^2}\left(\dfrac{dA}{dx}\right)^2 + \dfrac{1}{4\pi A}\left(\dfrac{dA}{dx}\right)^2\right] & \dfrac{dA}{dx} < 0, \end{cases} \tag{28}$$

$$u_r = \begin{cases} 0 & \dfrac{dA}{dx} \geq 0, \\ \dfrac{u_o A_o}{2A^2}\dfrac{dA}{dx} r & \dfrac{dA}{dx} < 0, \end{cases} \tag{29}$$

where it has been assumed that the material is rigid and exhibits bulk homogeneous flow in constant-area portions of the channel. Note that these equations imply that discontinuities in the velocity field can exist whenever there are discontinuities in the slope of the area function $A(x)$. However, in most practical cases the area gradients are small. These effects are therefore negligible (see Ref. 15) and will not be considered.

The stress field within the extruding material can be evaluated from Eqs. (8)–(11) by differentiating Eqs. (28) and (29) and once again neglecting higher order terms in $\frac{1}{A}(\frac{dA}{dx})^2$. The resulting equations are

$$s_{rr} = s_{\theta\theta} = \begin{cases} 0 & \dfrac{dA}{dx} \geq 0, \\ \dfrac{-Y}{3}\left[1 + \dfrac{r^2 g^2}{12}\right]^{-1/2} + \dfrac{\eta u_o A_o}{2A^2}\dfrac{dA}{dx} & \dfrac{dA}{dx} < 0, \end{cases} \tag{30}$$

$$s_{xx} = \begin{cases} 0 & \dfrac{dA}{dx} \geq 0, \\ \dfrac{2Y}{3}\left[1 + \dfrac{r^2 g^2}{12}\right]^{-1/2} - \dfrac{\eta u_o A_o}{A^2}\dfrac{dA}{dx} & \dfrac{dA}{dx} < 0, \end{cases} \tag{31}$$

$$s_{xr} = \begin{cases} 0 & \dfrac{dA}{dx} \geq 0, \\ \dfrac{-Ygr}{6}\left[1 + \dfrac{r^2 g^2}{12}\right]^{-1/2} + \dfrac{\eta u_o A_o}{4A^2}\dfrac{dA}{dx} gr & \dfrac{dA}{dx} < 0, \end{cases} \tag{32}$$

where coefficient of plastic deformation λ is given by

$$\lambda = \frac{\dot{\epsilon}_{eq}}{Y} = \frac{3}{2Y}\left|\frac{u_o A_o}{A^2}\frac{dA}{dx}\right|\left[1 + \frac{r^2 g^2}{12}\right]^{1/2}, \tag{33}$$

and g, given by

$$g = \left[\frac{-4}{A}\frac{dA}{dx} + \left(\frac{d^2A}{dx^2}\Big/\frac{dA}{dx}\right)\right], \tag{34}$$

will be referred to as the plastic deformation function. By substituting the value for s_{rr} given by Eq. (30) into Eq. (26) and making the appropriate first-order approximations, the frictional body force per unit volume may also be re-expressed as

$$f_f = \begin{cases} 0 & \dfrac{dA}{dx} \geq 0\,, \\ S(u_o)2\mu\sqrt{\dfrac{\pi}{A}}\left[\dfrac{-Y}{3} + \dfrac{\eta u_o A_o}{2A^2}\dfrac{dA}{dx} - p\right] & \mu\left|\dfrac{-Y}{3} + \dfrac{\eta u_o A_o}{2A^2}\dfrac{dA}{dx} - p\right| < \dfrac{mY}{\sqrt{3}}\,,\ \dfrac{dA}{dx} < 0\,, \\ -S(u_o)2m\sqrt{\dfrac{\pi}{3A}}\,Y & \mu\left|\dfrac{-Y}{3} + \dfrac{\eta u_o A_o}{2A^2}\dfrac{dA}{dx} - p\right| \geq \dfrac{mY}{\sqrt{3}}\,,\ \dfrac{dA}{dx} < 0\,, \end{cases} \tag{35}$$

where the coefficient of friction μ in this equation is given by Eq. (27). Then, by using the axial momentum equation, taking derivatives of the axial and radial velocity components, neglecting the higher-order area-gradient contributions to these terms, and removing any radial dependencies by evaluating the cross-sectional integral averages of the radial dependent terms, the inertia terms of the left-hand side of Eq. (3) can be expressed as

$$\frac{\partial u_x}{\partial t} + u_r\frac{\partial u_x}{\partial r} + u_x\frac{\partial u_x}{\partial x} \approx \frac{du_o}{dt}\frac{A_o}{A} - \frac{u_o^2A_o^2}{A^3}\frac{dA}{dx}\left[1 + \frac{1}{4\pi A}\left(\frac{dA}{dx}\right)^2\right]. \tag{36}$$

The surface forces found on the right-hand side of the axial momentum equation can then be rewritten by taking the derivatives of Eqs. (30)–(32) for the four components of stress, assuming that $rg/12 \ll 1$ (a good approximation if $\frac{1}{A}(\frac{dA}{dx})^2$ is small), keeping only the first-order terms, assuming that the only axial body force f_x acting on the extruding material is the frictional body force f_f defined by Eq. (35), and finally noting that the mean stress is merely the negative of the hydrostatic pressure. The resulting expression is

$$\frac{1}{\rho}\left[\frac{\partial s_{xx}}{\partial x} + \frac{\partial s_{xr}}{\partial r} + \frac{s_{xr}}{r}\right] + \frac{1}{\rho}\left[f_x + \frac{\partial \sigma_m}{\partial x}\right] \approx \frac{-Yg}{3\rho} - \frac{\eta u_o A_o}{2\rho A^2}\frac{d^2A}{dx^2} + \frac{1}{\rho}\left[f_f - \frac{\partial p}{\partial x}\right]. \tag{37}$$

Finally, by combining Eqs. (36) and (37), integrating the entire differential equation with respect to the position x from the back face of the extruding material x_b to the front face at location x_f, and then solving for $\frac{du_o}{dt}$, an ordinary differential equation can be obtained. It can be written as

$$\begin{aligned} \frac{du_o}{dt} = {} & \left[\frac{u_o^2A_o}{2A_b^2}\left(1 - \frac{A_b^2}{A_f^2}\right) + \frac{u_o^2A_o}{4\pi}\int_{x_b}^{x_f}\frac{1}{A^4}\left(\frac{dA}{dx}\right)^3 dx + \frac{p_b - p_f}{\rho A_o} - \frac{Y}{3\rho A_o}\int_{x_b}^{x_f} g\,dx \right. \\ & \left. - \frac{\eta u_o}{2\rho}\int_{x_b}^{x_f}\frac{1}{A^2}\frac{d^2A}{dx^2}\,dx + \frac{1}{\rho A_o}\int_{x_b}^{x_f} f_f\,dx\right]\left[\int_{x_b}^{x_f}\frac{dx}{A}\right]^{-1}, \end{aligned} \tag{38}$$

where the variables p_b and p_f represent the values of the instantaneous external pressures that are applied to the back and front faces of the extruding material and A_f and A_b are the respective areas. This completes the extrusion analysis.

The velocity field of the extruding material through axisymmetric dies is described by Eqs. (28) and (29). In turn, the internal stress field related to this velocity field is defined by Eqs. (30)–(34). Equations (27) and (35) define the equivalent frictional body force acting on the extruding material. Finally, Eq. (38) governs the evolution of the velocity field in time. The variable u_o of this ordinary differential equation represents the quasi-steady reference velocity in a section of the die with a fixed area A_o. This last equation relates the time rate of change of the reference velocity (i.e., acceleration of the extrudite) to the deformation forces acting on the body.

The numerator of Eq. (38) is a sum of six different terms, each related to various forcing mechanisms. The first two terms of the numerator represent the inertial forces and reflect the material's resistance to acceleration. They correspond to the axial and radial contributions to the inertial forces, respectively. The third term of the numerator is related to the normal surface forces acting on the front and back faces of the extruding material. This term specifies the external load or force which is actually forcing the material through the channel.

The fourth and fifth terms in the numerator of Eq. (38) reflect the shear surface forces retarding the motion. The first term that is proportional to the ultimate tensile yield strength of the material represents the surface shear forces due to ideal-plastic deformation. For conical area transitions, this term becomes a natural logarithmic function of the front- to back-face area ratio which is similar to the expressions of Hoffman and Sachs [6], Avitzur [1–3], and Cristescu [14, 15]. The second of these two shear-stress terms accounts for the strain rate effects due to the *viscosity* of the material. The influence of this term is normally significant even for low-speed extrusions.

The last term in the numerator of Eq. (38) accounts for the forces of friction between an extruding material and channel wall. It is the sum of the frictional body forces per unit volume, defined by Eq. (35), integrated over the entire length of the material. In many extrusion processes, the frictional forces can dominate.

In comparison to the original set of partial differential equations, it should be fairly obvious that the ordinary differential equation and related expressions of the preceding one-dimensional ideal-viscoplastic extrusion model are considerably easier to solve. Conventional numerical methods such as multi-step finite-differences or Runge-Kutta techniques can be used to integrate Eq. (38).

COMPARISON TO POLYETHYLENE EXTRUSION EXPERIMENTS

Validation of the one-dimensional ideal-viscoplastic extrusion model was sought by comparing predicted solutions to both experimental data and sophisticated two-dimensional finite-element computations. Some typical results of the experimental comparisons are presented in this section. Other results of the comparisons to finite-element predictions follow in the next section. See Groth, Gottlieb, and Bourget [33] for further comparisons.

Two different types of comparisons were made between the ideal-viscoplastic extrusion model and experiment. In the first type, the predicted forces of extrusion for cylindrical bodies in conical converging channels were compared to experimental measurements of these forces. In the second

type, the locally-spherical velocity field of the model was compared to experimental flow fields observed with the aid of a flow visualization technique.

Experimental measurements of extrusion forces were acquired from a set of low-speed extrusion tests with high-density polyethylene. Cylindrical samples of the polyethylene were extruded at constant back-face velocities by a high-pressure press through a two-stage conical die. The cylinders were 11.43 cm long and 3.175 cm in diameter. The die consisted of two conical area-reductions with the first having a convergence angle of 0.30° and the second having a convergence angle of 32° (see Fig. 5). During each extrusion, the position of the back face and the corresponding applied force were measured. This provided force data as a function of back-face position.

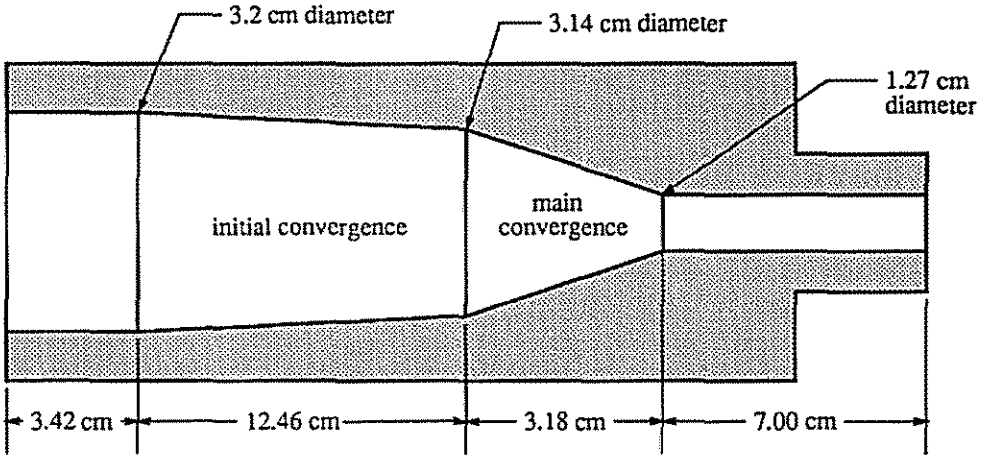

Fig. 5. Die used in polyethylene extrusion experiments.

The flow field or strain-rate distribution within the polyethylene was also visualized and mapped during the experiments by using visioplasticity, a useful flow-visualization technique developed during the 1950s [4, 9, 34]. In this technique, the undeformed cylinders were marked with a series of intersecting grid lines. The internal grids were generated by drilling small holes into the material and staining the holes with black ink. The holes were made in the axial-radial planes of the cylinders, in both axial and radial directions. After extrusion, the polyethylene samples were removed from the die and cut along the axial-radial plane containing the holes, thus revealing the distorted grids. By carefully examining the deformed grids, the predicted and experimental flow fields could be compared. This provided a method for substantiating the use of the kinematically-admissible locally-spherical velocity field in the extrusion model.

The predicted results for all of these experimental comparisons were obtained by numerically solving the equations for the ideal-viscoplastic extrusion model. A simple finite-difference time-stepping scheme was employed. The material constants of the high-density polyethylene used in these simulations were taken from material tests and manufacturer specifications ($\rho = 950$ kg/m^3, $Y = 21$ MPa, $\eta = 2.5$ MPa-s, $m = 1$, $\mu_s = 0.1$, and $\mu_k = \beta = 0$).

Experimental measurements and ideal-viscoplastic model predictions of the forces required to extrude polyethylene samples through the die at constant velocities of 0.17 mm/s and 19.1 mm/s and shown in Fig. 6. The force is depicted as a function of the back-face position. The zero value

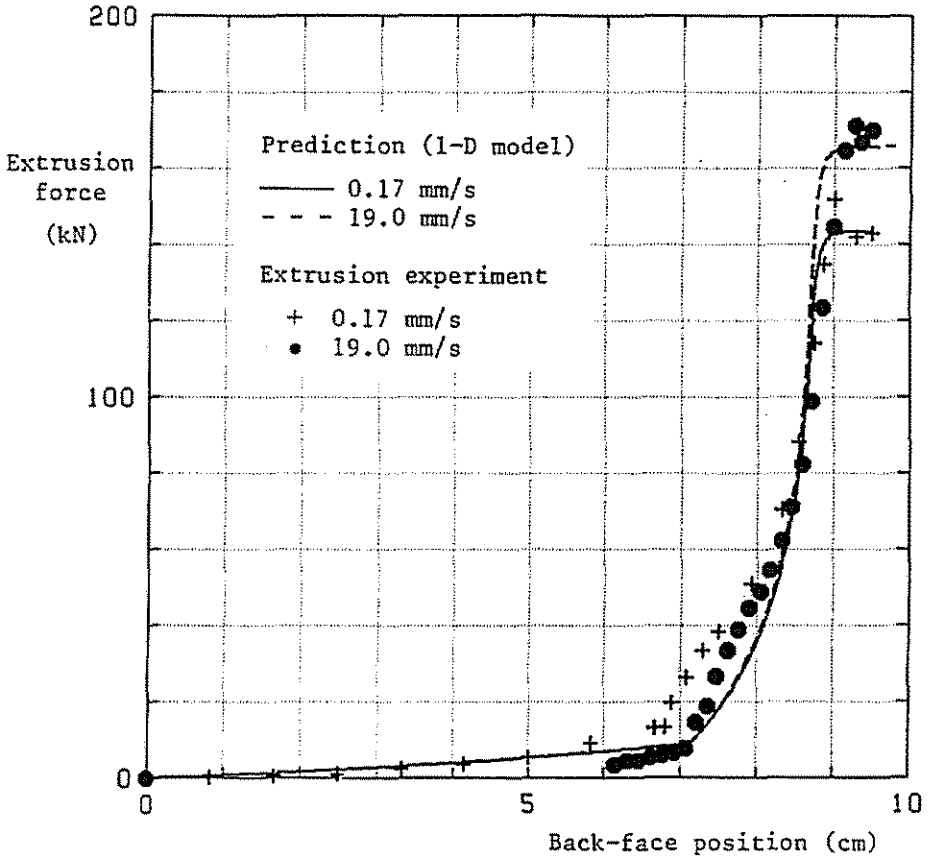

Fig. 6. Comparison of predicted and measured back-face forces for extrusion of polyethylene piston.

of the position coordinate represents the location at which the front face is at the entrance to the two-stage conical area reduction.

These results reveal that the experimental data and predictions of the ideal-viscoplastic model exhibit the same trends. Both sets of data indicate an increasing extrusion forces as the cylinders enter farther into the die and in both cases this forces reach an upper limit when the front face exits the die. Both sets of data appear to have slope discontinuities at the same three positions of the cylinder back face. These represent locations where the front face enters the first conical transition, enters the second conical transition, and exits the entire two-stage area reduction. In addition, the magnitudes of the analytic and experimental values of the maximum forces appear to be in agreement to within 10%.

It is instructive to compare the maximum extrusion forces from both extrusion trials. The maximum force of 170 kN measured in the higher-speed (19.1 mm/s) trial is much larger than the maximum force of 140 kN from the low-speed (0.17 mm/s) case. The agreement between prediction and experiment for these two cases indicates that the model can adequately represent combined inertial effects and strain-rate behaviour.

Some results of the visioplasticity experiments are depicted in Fig. 7. The distorted grids of three different extrusions corresponding to three back-face velocities of 0.17, 8.5, and 19.1 mm/s are shown. An examination of these deformed grids reveals a number of qualitative features of the

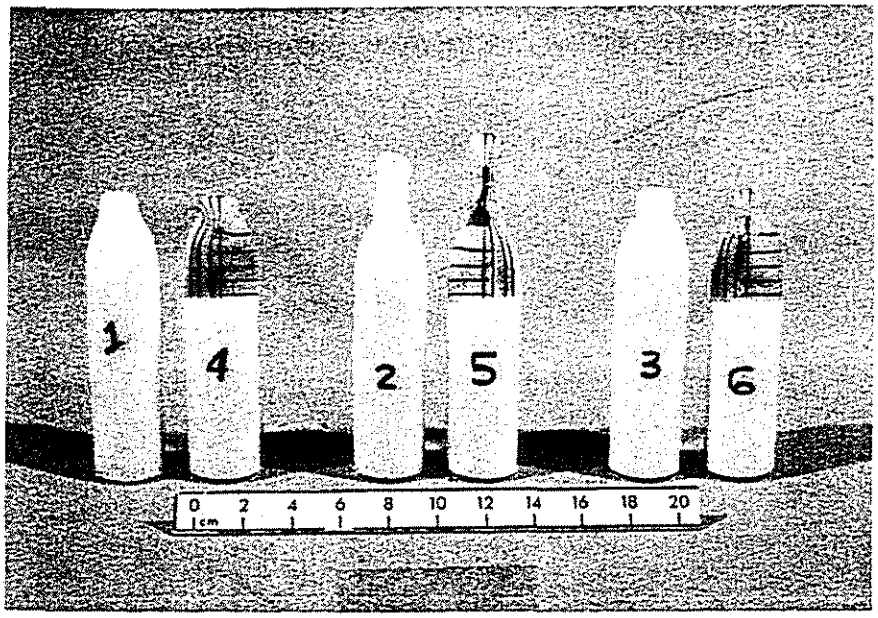

Fig. 7. Three sets of polyethylene samples from visioplasticity extrusion experiments illustrating grid distortion.

experimental flow fields that can then be compared to the predicted flow fields of the ideal-viscoplastic model.

Firstly, all of the distorted grids shown in the photograph have the same general characteristic shape and geometry, even though the back-face velocities were different in each case. This observation substantiates to some extent one of the important assumptions of the present analysis: flow fields of extrusions are geometrically similar and can be approximated by a quasi-steady kinematically-admissible velocity field.

Further observation reveals that the grids of the cylindrical polyethylene samples have been compressed. The compression seems to be greater toward the perimeter of the cylinders. This indicates that the experimental radial velocity component is negative and has a maximum magnitude near the walls of the die. Equation (29) describes the radial component of the locally-spherical velocity field. It predicts that this velocity component is zero at the axis of symmetry of the deforming material and linearly decreases to a minimum negative value at the channel wall. Equation (30) describes the radial component of the deviatoric normal stress produced by the radial strain rate. It predicts that the radial stress is compressive throughout the extruding body. It would seem that the behaviours of the radial velocity and stress components prescribed by Eqs. (29) and (30) agree with the experimental observations.

It is also apparent from the photograph that those radial grid lines which have entered the die have become wider and have curved forward. The curvature of the radial grid lines indicates that the axial velocity component of the experimental flow fields is radially dependent and has a magnitude that is maximum near the die walls. It also illustrates that slip occurs between the extruding material and die. This type of behaviour is also predicted by Eq. (28) describing the axial component of the locally-spherical velocity field. The widening of the grid lines indicates that

the experimental stress field has tensile components of axial stress. Axial tension is predicted by Eq. (31).

COMPARISON TO FINITE-ELEMENT COMPUTATIONS

The predictions of the one-dimensional ideal-viscoplastic extrusion model were also compared to two-dimensional finite-element-method computations. In this second set of comparisons, the ideal-viscoplastic model and finite-element solutions to various hypothetical piston extrusion problems were studied. From the detailed information provided by the finite-element computations, it was possible to investigate and substantiate many aspects of the extrusion model, including its emulation of the flow field, internal stresses, frictional forces, and strain-rate behaviour. Some typical results of the comparisons for one extrusion problem are now presented. Additional results may be found elsewhere (see Ref. 33).

The hypothetical extrusion problem can be described as follows. A 2.54-cm-diameter piston initially 1.5-m long with a density and ultimate yield strength of 1000 kg/m^3 and 10 MPa is extruded through a 2.0 m long conical die. The coefficient of viscosity for the material is assumed to be 10 MPa-s and the coefficient of friction is set to 0.01. The area-reduction ratio (entrance to exit area) and included angle of the die are 6.25 and 4.4°, respectively. The extrusion force applied to the back face is increased as the piston moves further into the area reduction in order to maintain a constant back-face velocity of 10 m/s.

The ideal-viscoplastic model solution to this hypothetical extrusion problem was again obtained by using a finite-difference time-stepping procedure. The finite-element solution to this same problem was obtained with the aid of the HONDO III computer program (refer to Ref. 18 for further details). The HONDO III computer program is a powerful finite-element-method code designed to calculate the large deformation, elastic and inelastic, transient response of two-dimensional and axisymmetric solids.

An axisymmetric, 64-element, 85-node, finite-element representation of the extruding piston was used. Although it is not possible to model exactly the ideal-viscoplastic behaviour of a Bingham body with the HONDO III software, the computer program can reproduce similar strain-rate-sensitive response by using the classical Prandtl-Reuss equations for elastic-plastic deformations [4, 6, 7, 10, 12, 19, 21, 26], in conjunction with the power-law relation between the strain rate and dynamic overstress of Symonds and Ting [25]. Note that this particular set of constitutive relationships incorporates the effects of elastic deformation. This was useful because it meant that the implications of neglecting elastic deformation in the approximate extrusion analysis could be appraised. A Young's modulus and Poisson's ratio of 90 MPa and 0.49 were used to represent the elastic response of the piston. Finally, the HONDO III finite-element code has provisions for including the frictional shear stresses created by two surfaces in sliding contact. This feature was used to model the effects of friction between the extruding material and the die.

Some results for both the one-dimensional ideal-viscoplastic model and HONDO III finite-element-method solutions to the hypothetical extrusion problem are compared in the graphs of Figs. 8 and 9. The front-face position and velocity as well as the back-face extrusion pressure required to maintain a constant back-face velocity are all plotted as functions of the back-face position in Fig. 8. Spatial distributions of the stress field at a fixed instance in time during the

extrusion process are given in Fig. 9. The initial position of the piston back face (i.e., $x = 0$) represents a location where the front face of the undeformed piston is situated at the entrance to the die.

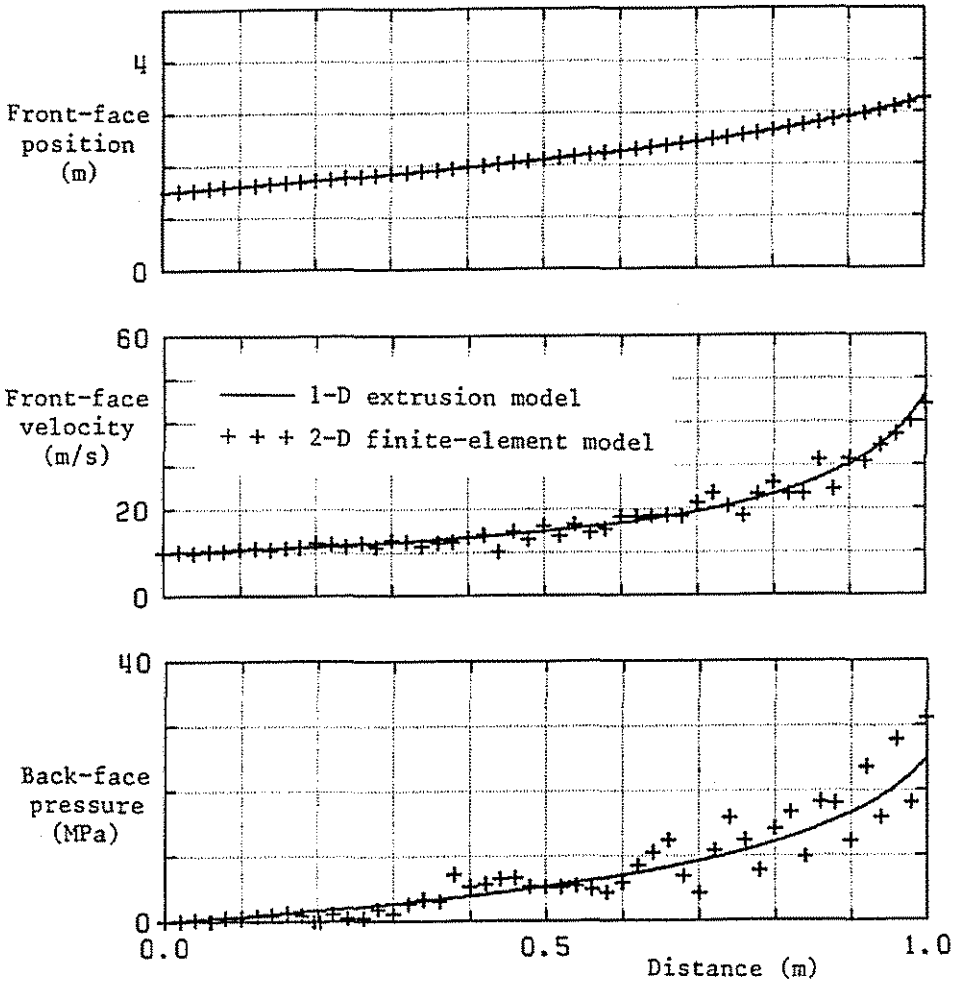

Fig. 8. Comparison of predicted motion and extrusion force of ideal-viscoplastic extrusion model and HONDO III finite-element code (extrusion speed 10 m/s, frictional forces included).

The approximate model and finite-element-method predictions of the front-face position and velocity as function of the location of the back face, as shown in Fig. 8, are in agreement. This should be expected for an incompressible material. Of more interest is the plot of the back-face pressure also shown in the figure. As the piston moves farther into the die and more deformation occurs, the back-face pressure required to maintain a constant back-face velocity increases. The one-dimensional solution for the deformation forces closely approximates the predictions of the more sophisticated two-dimensional finite-element program, suggesting that the simplified model's predictions of the plastic, strain-rate dependent, and friction forces are quite valid. Note that the predicted pressures of the HONDO III program oscillate about the results of the simplified model. These oscillations may be attributed mainly to unsteady elastic wave motion that is included in the

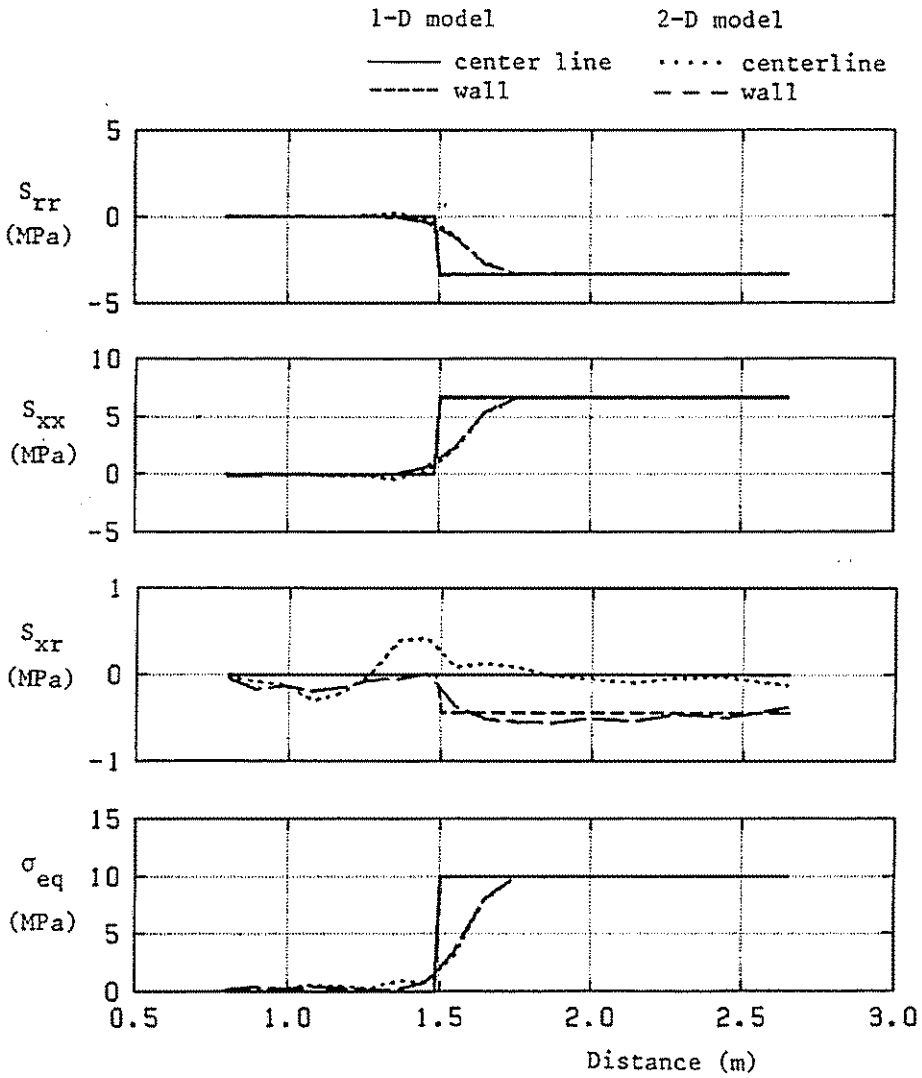

Fig. 9. Comparison of predicted stresses of ideal-viscoplastic extrusion model and HONDO III finite-element code (extrusion speed 10 m/s, frictional forces included).

finite-element solution but neglected in the approximate one.

The distributions of the radial and axial components of deviatoric normal stress, shear stress in the axial-radial plane, and equivalent stress, all evaluated along the axis of symmetry ($r = 0$) and the wall of the die, are shown at time $t = 80$ ms in Fig. 9. At this time, the front face of the piston is located approximately two-thirds of the way into the die. Back and front faces of the piston are indicated by the start and finish of the curves.

A number of observations can be made from these stress distributions. First of all, the ideal-viscoplastic model and finite-element predictions of axial and radial components of deviatoric normal stress, shear stress in the axial-radial plane, and equivalent stress are very similar. Both sets of

results have similar characteristics and the magnitudes of the predicted stresses are in agreement. Note that s_{rr} is negative, indicating compression in the radial direction, and s_{xx} is positive, indicating tension in the axial direction.

Secondly, the finite-element solutions of Fig. 9, particularly the results for equivalent stress, indicate that majority of the piston material in the die is undergoing plastic deformation. The portion of the piston undergoing elastic deformation is not significant. This indicates that ideal-viscoplastic constitutive relations, which neglect elastic deformation, are very appropriate for this type of extrusion problem.

One final observation concerns the one-dimensional nature of the extrusion process. The plots of the finite-element predictions of radial and axial deviatoric stress and equivalent stress calculated along the axis of symmetry and wall are virtually indistinguishable. This indicates that the two-dimensional extrusion process has many one-dimensional characteristics and suggests that one-dimensional models may be used to represent the process. However, the curves depicting the shear stress at $r = 0$ and along the wall show that this stress is radially dependent. Thus, one-dimensional models of the extrusions must reflect this two-dimensional feature. Judging from the plot of the shear stress distributions, the approximate one-dimensional model adequately includes this important two-dimensional effect.

CONCLUDING REMARKS

An approximate solution procedure for extrusions of ideal-viscoplastic material through rigid axisymmetric dies has been presented. This unsteady one-dimensional model incorporates the fundamental two-dimensional features of extrusions, including the effects of inertia, plastic strain, strain rate, and surface friction, into a cohesive analysis that does not require complicated numerical solution techniques. The analysis can be viewed as an extension and generalization of the work of Cristescu [14, 15] to include inertial terms and a more sophisticated friction model, as well as to allow the treatment of axisymmetric channel geometries.

The solutions of the ideal-viscoplastic model were carefully compared to other experimental and finite-element-method results for a number of extrusion problems. The predictions of the one-dimensional model were found to agree well with the experimental and finite-element data.

Although the approximate model is valid only for incompressible materials that exhibit ideal-viscoplastic deformation response and cannot predict unsteady wave motion within the material, non-viscoplastic material response, and special flow field anomalies and irregularities such as shaving, central-bursting, and dead-zone formation [1–3], many practical extrusion processes may be simulated. Furthermore, the analysis is an ideal tool for design optimization procedures or other uses where computational times must be minimized. It has already been used successfully to predict the extrusion of high-density polyethylene pistons in the area convergences between pump and launch tubes of two-stage light-gas hypervelocity launchers [35–37].

ACKNOWLEDGMENTS

Financial support for this research was received from the Defense Research Establishment Valcartier (DREV), Courcelette, Quebec, Canada, under DSS Contract Serial No. 8SD85-00145. The experiments were conducted at DREV and the authors are grateful to Mr. C. Bourget for

his help in this matter. Finally, the authors would also like to thank Mr. E. Skiba and Mr. M. Lafreniere of the Ontario Research Foundation (ORF), Mississauga, Ontario, Canada for performing the HONDO III finite-element predictions.

REFERENCES

1 Avitzur B., *Metal Forming: Processes and Analysis*, McGraw-Hill, Toronto, 1968.

2 Avitzur B., *Study of Flow Through Conical Converging Dies*, Metal Forming: Interrelation Between Theory and Practice (Ed: Hoffmanner, A.L.), Plenum Press, New York, pp. 1–46, 1971.

3 Avitzur B., *Handbook of Metal-Forming Processes*, John Wiley, Toronto, 1983.

4 Dieter G.E., *Mechanical Metallurgy*, McGraw-Hill, Toronto, 1976.

5 Michaeli, W., *Extrusion Dies: Design and Engineering Computations*, Hanser Publishers, New York, 1984.

6 Hoffman O., and Sachs G., *Introduction to the Theory of Plasticity for Engineers*, McGraw-Hill, New York, 1953.

7 Hill R., *The Mathematical Theory of Plasticity*, Oxford University Press, London, 1950.

8 Johnson W., *Extrusion Through Square Dies of Large Reduction*, J. Mech. Phys. Solids 4, pp. 191–198, 1956.

9 Jordan T.F., and Thomsen E.G., *Comparison of an Unsymmetric Slip-Line Solution in Extrusion with Experiment*, J. Mech. Phys. Solids 4, pp. 184–190, 1956.

10 Prager W., and Hodge P.G., *Theory of Perfectly Plastic Solids*, John Wiley and Sons, New York, 1951.

11 Shield R.T., *Plastic Flow in a Converging Conical Channel*, J. Mech. Phys. Solids **3**, pp. 246–258, 1955.

12 Martin J.B., *Plasticity*, The MIT Press, Cambridge, 1975.

13 Leech C., *Piston Extrusion in Light-Gas Guns*, CARDE Tech. Rept. 580/67, November 1967.

14 Cristescu N., *Plastic Flow Through Conical Converging Dies Using A Viscoplastic Constitutive Equation*, Int. J. Mech. Sci. **17**, pp. 425–433, 1975.

15 Cristescu N., *Drawing Through Conical Dies — An Analysis Compared with Experiments*, Int. J. Mech. Sci. **18**, pp. 45–49, 1976.

16 Zienkiewicz O.C., and Cheung Y.K., *The Finite Element Method in Structural and Continuum Mechanics*, McGraw-Hill, New York, 1967.

17 Zienkiewicz O.C., *The Finite Element Method*, McGraw-Hill, Toronto, 1977.

18 Key S.W., *A Finite Element Procedure for the Large Deformation Dynamic Response of Axisymmetric Solids*, Comp. Methods Appl. Mech. Eng. 4, pp. 195–218, 1974. Also, Key S.W., *HONDO, A Finite Element Computer Program for the Large Deformation Dynamic Response of Axisymmetric Solids*, Research Rept. SLA-74-0039, Sandia Laboratories, Albuquerque, New Mexico, January 1974.

19 Blazynski T.Z., *Applied Elasto-Plasticity of Solids*, MacMillan, London, 1983.

20 Schlichting H., *Boundary Layer Theory*, Pergamon Press, New York, 1955.

21 Cristescu N., *Dynamic Plasticity*, North-Holland Publishing, Amsterdam, 1967.

22 Kraus H., *Two-Dimensional Analysis of a Hypervelocity Impact Upon a Visco-Plastic Plate*, Proc. Sixth Symp. Hypervelocity Impact III, pp. 14–40, August 1963.

23 Riney T.D., and Chernoff P.R., *Inertial, Viscous, and Plastic Effects in High High Speed Impact*, Proc. Fifth Symp. Hypervelocity Impact I, pp. 135–162, April 1962.

24 Riney T.D., *Visco-Plastic Solution of Hypervelocity Impact Cratering Phenomenon*, Proc. Sixth Symp. Hypervelocity Impact II, pp. 105–140, August 1963.

25 Symonds P.S., and Ting T.C.T., *Longitudinal Impact on Viscoplastic Rods — Approximate Methods and Comparisons*, ASME J. Appl. Mech. **31**, pp. 611–620, 1964.

26 Mendelson A., *Plasticity: Theory and Application*, Macmillan, New York, 1968.

27 Sechler E.E., *Elasticity in Engineering*, Dover Publications, New York, 1968.

28 Kragelsky I.V., Dobychin M.N., and Kombalov V.S., *Friction and Wear Calculation Methods*, Pergamon Press, Toronto, 1982.

29 Palmer F., *What About Friction?*, Amer. J. Phys. 17(6), pp. 181–187 & 327–342, 1949.

30 Bowden F.P., and Freitag E.H., *The Friction of Solids at Very High Speeds: I. Metal on Metal; II. Metal on Diamond*, Proc. Royal Soc. London–A **248**, pp. 350–367, 1958.

31 Powell E.S., Winstead C.A., DeWitt J.R., and Cable A.J., *A Preliminary Study of Model Wear in a Two-Stage Light-Gas Launcher*, 36th meeting of the Aeroballistic Range Association, San Antonio, Texas, October 1985.

32 Powell E.S., DeWitt J.R., and Cable A.J., *Further Study of Model Wear in a Two-Stage Light-Gas Launcher*, 37th meeting of the Aeroballistic Range Association, Quebec, Quebec, September 1986.

33 Groth C.P.T., Gottlieb J.J., and Bourget C., *Ideal-Viscoplastic Extrusion Model with Application to Deforming Pistons in Light-Gas Guns*, UTIAS Tech. Note No. 266, University of Toronto, November 1987.

34 Medrano, R., Gillis, P., Hinesley, C., and Conrad, H., *Application of Visioplasticity Techniques to Axisymmetric Extrusions*, Metal Forming: Interrelation Between Theory and Practice (Ed: Hoffmanner, A.L.), Plenum Press, New York, pp. 85–104, 1971.

35 Groth C.P.T. and Gottlieb J.J., *Numerical Study of Two-Stage Light-Gas Hypervelocity Projectile Launchers*, UTIAS Rept. No. 327, University of Toronto, October 1988.

36 Gottlieb, J.J., Groth, C.P.T., Lesage, F., and Maillette, J., *Numerical Model for Prediction of Two-Stage Light-Gas Gun Performance*, Proc. 11th Int. Symp. Ballistics, Vol. I, pp. 445–455, Brussels, Belgium, May 1989.

37 Matsumura T., Takayama, K., and Gottlieb, J.J., *A Numerical Study of the Performance of a Two-Stage Light-Gas Gun*, Trans. JSME Part B **526**, pp. 142–145, 1990.

NOMENCLATURE

A	channel cross-sectional area (m^2)
A_b	back-face cross-sectional area of the extrudite (m^2)
A_f	front-face cross-sectional area of the extrudite (m^2)
A_o	reference cross-sectional area (m^2)
f_f	axial frictional body force per unit volume ($kg/m^2 \cdot s^2$)
f_r	radial component of the body force per unit volume ($kg/m^2 \cdot s^2$)
f_x	axial component of the body force per unit volume ($kg/m^2 \cdot s^2$)
g	plastic deformation function (m^{-1})
m	maximum frictional shear stress proportionality constant
p	pressure (Pa)
p_b	pressure at the back face of the extrudite (Pa)
p_f	pressure at the front face of the extrudite (Pa)
r	radial component of axisymmetric position coordinates (m)
R	radial component of spherical position coordinates (m)
s_{ij}	generalized deviatoric stress tensor (Pa)
s_{rr}	radial component of deviatoric normal stress (Pa)
s_{xx}	axial component of deviatoric normal stress (Pa)
$s_{\theta\theta}$	azimuthal component of deviatoric normal stress (Pa)
s_{xr}	deviatoric shear stress component (Pa)
t	time (s)
u_o	reference velocity (m/s)
u_r	radial component of velocity vector in axisymmetric coordinates (m/s)
u_x	axial component of velocity vector in axisymmetric coordinates (m/s)
u_R	radial component of velocity vector in spherical coordinates (m/s)
u_Φ	angular component of velocity vector in spherical coordinates (m/s)
u_Ψ	angular component of velocity vector in spherical coordinates (m/s)
V_o	reference velocity describing friction coefficient (m/s)

x	axial component of axisymmetric position coordinates (m)
Y	tensile yield stress (Pa)
α	semi-angle of conical area reduction
β	velocity decay parameter describing friction coefficient (s/m)
$\dot{\epsilon}_{eq}$	equivalent or effective strain rate (s^{-1})
$\dot{\epsilon}_{ij}$	generalized strain-rate tensor (s^{-1})
$\dot{\epsilon}_{rr}$	radial strain-rate component (s^{-1})
$\dot{\epsilon}_{xx}$	axial strain-rate component (s^{-1})
$\dot{\epsilon}_{\theta\theta}$	azimuthal strain-rate component (s^{-1})
$\dot{\epsilon}_{xr}$	shear strain-rate component (s^{-1})
η	viscosity coefficient for viscoplastic deformation (Pa·s)
θ	azimuthal component of axisymmetric position coordinates
λ	plastic deformation proportionality coefficient ($Pa^{-1}s^{-1}$)
μ	coefficient of friction
μ_k	kinematic coefficient of friction
μ_s	static coefficient of friction
ρ	density (kg/m^3)
σ_{eq}	equivalent or effective stress (Pa)
σ_{ij}	generalized stress tensor (Pa)
σ_m	mean or hydrostatic stress (Pa)
σ_n	normal stress (Pa)
σ_{rr}	radial component of normal stress (Pa)
σ_{xx}	axial component of normal stress (Pa)
$\sigma_{\theta\theta}$	azimuthal component of normal stress (Pa)
σ_{xr}	shear stress component (Pa)
Φ	azimuthal component of spherical position coordinates
Ψ	azimuthal component of spherical position coordinates